JOURNAL OF GUIDANCE, CONTROL, AND DYNAMICS
Vol. 23, No. 3, May–June 2000

Optimal Vibration Control of Thin-Walled Anisotropic Cantilevers Exposed to Blast Loadings

Sungsoo Na*
Korea Polytechnic University, Keongki-do 429-450, Republic of Korea
and
Liviu Librescu†
Virginia Polytechnic Institute and State University, Blacksburg, Virginia 24061-0219

A study of optimal feedback control of the dynamic response of cantilevers exposed to blast loadings is presented. The structure to be controlled consists of a thin-walled beam of closed cross section contour that encompasses a number of nonclassical features such as transverse shear, primary and secondary warping, and anisotropy of the constitutent material. The control is achieved via the use of actuating and sensing capabilities provided by piezoelectric devices that are bonded or embedded into the host structure. In addition, the directionality property of advanced fiber-reinforced composite materials is also used to tailor the host structure to obtain an enhanced dynamic response. The cases of piezoactuators spread over the entire span of the structure or in the form of a patch are considered, and issues related with the influence of patch location and size on the control efficiency are discussed. Other issues related to the minimization of the required input power and implications of the limitation of control input voltage and of those generated by the inclusion/discard in the quadratic performance index of time-dependent external excitations are also addressed.

I. Introduction

THE increasing need for high-speed, highly flexible, and lightweight structural flight vehicles, capable of operating in severe environmental conditions, has prompted the development of a new concept in the modeling, analysis, and control of structures. This concept is based on the extensive use of advanced composite material structures[1] and integration in their construction of smart materials technology.[2] Such structures are often called intelligent/smart composite material structures.

As smart materials, the piezoelectric elements are successfully used in the feedback control of structures. Among the attributes contributing to their widespread use in control applications are the efficient conversion of electrical to mechanical energy, the ability to perform shape control, and the mechanical simplicity of the actuator. Whereas the sensing capability is achieved through the direct piezoelectric effect consisting of the generation of electrical charge due to the input strains, the actuating capability is achieved through the converse piezoelectric effect, which consists of the generation of localized strains in response to an applied voltage. This induced strain field produces, in turn, a change in the dynamic response characteristics of the structure. Implementation of a control law relating the applied electric field with one of the kinematical response quantities of the host structure according to a prescribed functional relationship results in a closed-loop boundary-value problem. However, to suppress the oscillations in the minimum possible time and with the minimum expenditure of energy, optimal control strategies have to be implemented.

Moreover, in view of the damaging effects the time-dependent loads might have on structural integrity and operational life of flight vehicle, adequate methodologies able to predict and control their dynamic response have to be devised and used.

Hererin both the optimal feedback control methodology and the directionality property of fibrous composites are used to control the dynamic response of cantilevered thin-walled beam structures to time-dependent external excitations. The cantilevered beams can serve as a basic model for a number of structures used in the aeronautical and aerospace industries, such as airplane wings, helicopter blades, robotic manipulator arms, and space booms, as well as other technological applications.

As for time-dependent loads, these can be induced by nuclear blast, gust, sonic boom, shock wave, fuel explosion, etc. Implementation in such sensitive structural systems of advanced capabilities to control their dynamic response to time-dependent external loads constitutes issues of vital importance toward prolonging their operational life and successful accomplishment of their mission.

II. Basic Statements

Two coordinate systems are used in the forthcoming developments: 1) a global rectangular system, (x, y, z), where x and y are the cross section beam coordinates and z is the spanwise coordinate, and 2) a local system (n, s, z), where n and s are the thickness coordinate normal to the beam midsurface and the tangential coordinate along the contour line of the beam cross section, respectively (see Fig. 1). The master structure is assumed to be composed of r anisotropic material layers, whereas the piezoactuators are assumed to exhibit symmetry properties with respect to the n axis, coinciding with the direction of polarization (rotary symmetry). As a result, the surface of isotropy of the piezoactuator is parallel at each point to the midsurface of the beam. In addition, it is supposed that piezoactuators are in the form of patches distributed along the circumferential, thickness, and spanwise directions, s, n, and z, respectively, according to the law

$$R_{(k)}(n) = Y(n - n_{k^-}) - Y(n - n_{k^+})$$

$$R_{(k)}(s) = Y(s - s_{k^-}) - Y(s - s_{k^+})$$

$$R_k(z) = Y(z - z_1) - Y(z - z_2) \tag{1}$$

In these equations $Y(\cdot)$ is the Heaviside distribution, R is a spatial function, and subscript k identifies the affiliation of the indicated quantity to the kth layers. In the limit, when $z_1 = 0$ and $z_2 = L$, the actuators become spread over the entire beam span.

To obtain the basic equations for the master structure, the following assumptions are adopted: 1) The cross sections of the beam do not deform in their own planes. 2) Transverse shear flexibility featured by the advanced composite material systems is taken into consideration. 3) The hoop stress resultant N_{ss} is negligibly small

Received 22 October 1998; revision received 5 September 1999; accepted for publication 6 September 1999.

*Assistant Professor, Department of Automation Engineering, Shiheung City; nass@kpu.ac.net.

†Professor, Engineering Science and Mechanics Department; librescu@vt.edu.

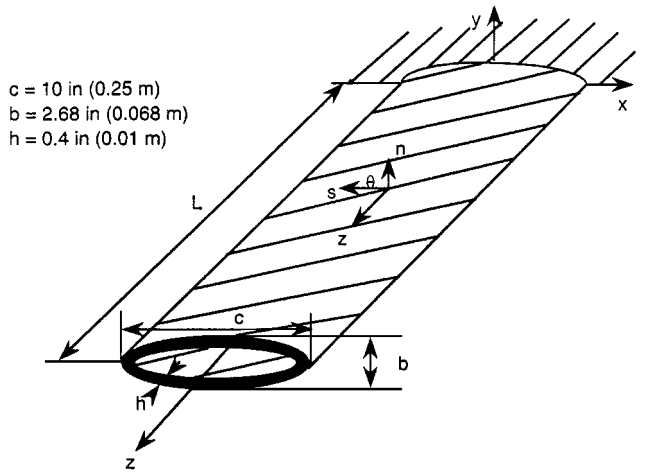

Fig. 1a Geometry of thin-walled beam.

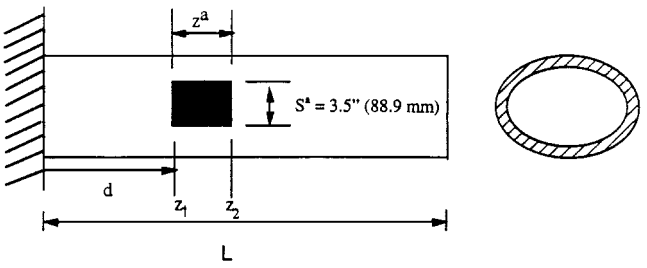

Fig. 1b Piezopatch configuration; piezoactuator thickness t^a = 0.00787 in.

compared to the remaining stress resultants. 4) Anisotorpy of constituent layer materials of the host structure is included in the model. 5) It is a nonuniform torsional model, in the sense that the rate of twist $d\Theta/dz$ is a function of the spanwise coordinate. 6) Primary and secondary warping effects are included in the structural model.

III. Governing System: Basic Equations

In view of the listed assumptions and of the results in Refs. 3–7, the strain measures assume the following form.

Axial strain:

$$S_{zz}(n, s, z, t) = \bar{S}_{zz}(s, z, t) + n\bar{\bar{S}}_{zz}(s, z, t) \tag{2a}$$

where

$$\bar{S}_{zz}(s, z, t) = w_0'(z, t) + \theta_y'(z, t)x(s) + \theta_x'(z, t)y(s) - \Theta''(z, t)F_\omega(s) \tag{2b}$$

and

$$\bar{\bar{S}}_{zz}(s, z, t) = \theta_y'(z, t)\frac{dy}{ds} - \theta_x'(z, t)\frac{dx}{ds} - \Theta''(z, t)a(s) \tag{2c}$$

are the axial strains associated with the primary and secondary warping, respectively.

Tangential shear strain:

$$S_{sz}(s, z, t) = \bar{S}_{sz}(s, z, t) + 2(A_C/\beta)\Theta'(z, t) \tag{3a}$$

where

$$\bar{S}_{sz}(s, z, t) = [\theta_y(z, t) + u_0'(z, t)]\frac{dx}{ds} + [\theta_x(z, t) + v_0'(z, t)]\frac{dy}{ds} \tag{3b}$$

Transverse shear strain:

$$S_{nz}(s, z, t) = [\theta_y(z, t) + u_0'(z, t)]\frac{dy}{ds} - [\theta_x(z, t) + v_0'(z, t)]\frac{dx}{ds} \tag{4}$$

In these equations and in the remainder of the paper, $(\cdot)' \equiv \partial(\cdot)/\partial z$.

In addition, $u_0(z, t)$, $v_0(z, t)$, $w_0(z, t)$, $\theta_y(z, t)$, $\theta_x(z, t)$, and $\Theta(z, t)$ are the translations in the x, y, and z directions and the rotations about the x, y, and z axes, respectively. These one-dimensional displacement measures are used to define the three-dimensional displacement vector of components u, v, and w in the x, y, and z directions, respectively. In the same equations, $F_\omega(s)$ is the primary warping function, A_c is the cross-sectional area bounded by the midline contour, β is the total length of the contour midline (see Refs. 3–7).

For the general case, $u_0(z, t)$, $v_0(z, t)$, and $w_0(z, t)$, and $\theta_x(z, t)$, $\theta_y(z, t)$, and $\Theta(z, t)$ constitute the basic unknown functions. When transverse shear is ignored, $\theta_x \to -v_0'$ and $\theta_y \to -u_0'$, and as a result, the number of unknowns reduce to only four independent quantities.

However, as is well known,[5,6] for aircraft wings, the bending–twist elastic coupling appears to be the most beneficial one, in the sense that it enables one to enhance their structural/aeroelastic response behavior.

As it was shown in Ref. 8, the ply-angle distribution with respect to the spanwise z axis inducing such a cross coupling is

$$\theta(y) = -\theta(-y) \tag{5}$$

Two distinct cases, case a) and case b), will be considered in the next developments: In case a the piezoactuator is constituted of a single patch of finite size distributed along the beam span, and in case b the piezoactuator is spread over the entire span of the beam. In both cases, the actuators are modeled as symmetric pairs mounted on the top and bottom external beam surfaces.

As a result of the implementation of the ply-angle scheme defined by Eq. (5), in view of the results obtained in Refs. 3–7 and of the out-of-phase actuation, the governing equations of the combined host–piezoactuator structure, written in an unified way for both cases a and b are as follows:

$$\delta v_0: \quad a_{55}(v_0'' + \theta_x') + \underline{a_{56}}\Theta''' + p_y = b_1\ddot{v}_0 \tag{6a}$$

$$\delta\theta_x: \quad a_{33}\theta_x'' + a_{37}\Theta'' - a_{55}(v_0' + \theta_x) - \underline{a_{56}}\Theta'' - \delta_P\hat{M}_x' = (\underline{b_4} + \underline{b_{14}})\ddot{\theta}_x \tag{6b}$$

$$\delta\Theta: \quad -\underline{a_{66}}\Theta'''' + a_{77}\Theta'' - a_{56}(v_0''' + \theta_x'') + a_{73}\theta_x'' = (b_4 + b_5)\ddot{\Theta} \tag{6c}$$

For cantilevered beams, the boundary conditions to be prescribed are as follows:

At $z = 0$,

$$v_0 = 0 \tag{7a}$$

$$\theta_x = 0 \tag{7b}$$

$$\Theta = 0 \tag{7c}$$

$$\underline{\Theta'} = 0 \tag{7d}$$

At $z = L$,

$$\delta v_0: \quad a_{55}\left(v_0' + \theta_x\right) + \underline{a_{56}}\Theta'' = 0 \tag{8a}$$

$$\delta\theta_x: \quad a_{33}\theta_x' + a_{37}\Theta' = \delta_S\hat{M}_x \tag{8b}$$

$$\delta\Theta: \quad -\underline{a_{66}}\Theta''' + a_{77}\Theta' - a_{56}\left(v_0'' + \theta_x'\right) + a_{37}\theta_x' = 0 \tag{8c}$$

$$\delta\Theta': \quad a_{56}\left(v_0' + \theta_x\right) + \underline{a_{66}}\Theta'' = 0 \tag{8d}$$

The terms underscored in Eqs. (6–8) by single and double dotted lines are associated with warping inhibition and rotatory inertia,

respectively. In the case of the Saint-Venant free warping model, the terms underscored by a single line become zero-valued quantities.

In the case of the material of the host structure featuring transversely isotropic properties, the bending and torsion motions become decoupled. Within such a special case, only the bending motion is considered. Details on the expressions of the stiffness quantities proper to this special case are supplied in Ref. 4.

For the infinitely rigid in transverse shear beam model, that is, for Bernoulli–Euler–Rayleigh structural model, Eqs. (6–8) modify as follows:

$$\delta v_0: \quad a_{33}v_0'''' - a_{37}\Theta''' - p_y + \delta_P \hat{M}_x'' = -b_1\ddot{v}_0 + \underline{(b_4 + b_{14})}\,\ddot{v}_0'' \tag{9a}$$

$$\delta\Theta: \quad \underline{-a_{66}\Theta''''} + a_{77}\Theta'' - a_{73}v_0''' + m_z = (b_4 + b_5)\ddot{\Theta} \tag{9b}$$

and the boundary conditions become, at $z = 0$,

$$\Theta = 0; \qquad \underline{\Theta'} = 0; \qquad v_0 = 0; \qquad v_0' = 0 \tag{10a–d}$$

and at $z = L$,

$$\delta v_0: \quad a_{33}v_0''' = \underline{(b_4 + b_{14})}\,\ddot{v}_0'' \tag{11a}$$

$$\delta v_0': \quad a_{37}\Theta' - a_{33}v_0'' = \delta_S \hat{M}_x \tag{11b}$$

$$\underline{\delta\Theta}: \quad \underline{-a_{66}\Theta'''} + a_{77}\Theta' - a_{37}v_0'' = 0 \tag{11c}$$

$$\delta\Theta': \quad \delta\Theta'' = 0 \tag{11d}$$

From Eqs. (6) and (9) it appears evident that, in the cases of shear deformable and infinitely rigid in transverse shear thin-walled beams, the governing equations exhibit the same order, namely, eight. As a result, in both cases the same number of boundary conditions, namely, four, has to be prescribed at each edge. A similar characteristic was noticed to exist also within the solid beam model (see Ref. 9).

In these equations, the tracers δ_P and δ_S take the values 1 or zero, depending on whether the actuator constitutes a piezopatch located along the beam span (in which case $\delta_P = 1$ and $\delta_S = 0$) or is spread over the entire span of the beam (which requires $\delta_S = 1$ and $\delta_P = 0$). Whereas in the former case the piezoelectrically induced moment occurs in the governing equation, in the latter one it intervenes in the boundary conditions at the beam tip, and as a result the control is achieved via the piezoelectrically induced boundary bending moment.

For the general case, the expression of the piezoelectrically induced bending moment is given by (see Ref. 6)

$$\hat{M}_x = \oint_C \sum_{k=1}^{\ell} \mathcal{E}_3^{(k)} \left(n_{(k^+)} - n_{(k^-)}\right) e_{31}^{(k)} R_{(k)}(s, z) \times \left[y\left(1 - \frac{A_{12}}{A_{11}}\right) + \frac{\mathrm{d}x}{\mathrm{d}s}\frac{B_{12}}{A_{11}} \right] \mathrm{d}s - \frac{1}{2}\oint_C \underline{\left[\frac{\mathrm{d}x}{\mathrm{d}s} \sum_{k=1}^{\ell} \mathcal{E}_3^{(k)} \left(n_{(k^+)}^2 - n_{(k^-)}^2\right) e_{31}^{(k)} R_{(k)}(s, z) \right]} \mathrm{d}s \tag{12}$$

where ℓ is the number of piezoelectric layers.

Equation (12) reveals that the piezoelectrically induced bending moment is proportional to the applied electric current $\mathcal{E}_3$. In the case of actuators symmetrically located through the thickness of the beam, the underlined term in Eq. (12) vanishes.

When the actuators are distributed over the entire beam span, $R(s, z) \Rightarrow R(s)$, and $\hat{M}_x$ becomes independent of the z coordinate. Consequently, its contribution in the governing equations becomes immaterial and, as a result, it appears in the boundary conditions only.

In contrast to this case, that is, when a piezoelectric patch is involved, $\hat{M}_x \equiv \hat{M}_x(z)$, and consequently its contribution appears solely in the governing equations.

In the case of piezoactuators constituted of a patch, the stiffness quantities a_{ij} and the mass terms b_i can be cast as

$$a_{ij} = \bar{a}_{ij} + \delta_P \hat{a}_{ij} + \delta_S \hat{\hat{a}}_{ij} \tag{13a}$$

$$b_i = \bar{b}_i + \delta_P \hat{b}_i + \delta_S \hat{\hat{b}}_i \tag{13b}$$

where the terms affected by an overbar and the circumflex signs are associated with the host structure and the piezoactuators, respectively. Their expressions are supplied in different contexts in Refs. 6 and 10.

Because the applied electric field $\mathcal{E}_3$ can be expressed as $V(t)/h$, in the case of a piezopatch, an alternative representation for the piezoelectrically induced bending moment is obtained as

$$\hat{M}_x(z, t) = \mathcal{C}V(t)[Y(z - z_1) - Y(z - z_2)] \tag{14}$$

where $\mathcal{C}$ is a constant dependent on the mechanical and geometrical properties of the piezoactuator and host structure whereas $V(t)$ is the applied input voltage (out-of-phase actuation).

IV. Discretized Boundary-Value Problem

To discretize the boundary-value problem, $v_0(z, t)$, $\theta_x(z, t)$, and $\Theta(z, t)$ will be represented as

$$v_0(z, t) = \boldsymbol{V}^T(z)\boldsymbol{q}_v(t), \qquad \theta_x(z, t) = \boldsymbol{R}^T(z)\boldsymbol{q}_R(t)$$
$$\Theta(z, t) = \boldsymbol{S}^T(z)\boldsymbol{q}_S(t) \tag{15}$$

where

$$\boldsymbol{V}(z) = [v_1, v_2, \ldots, v_N]^T, \qquad \boldsymbol{R}(z) = [r_1, r_2, \ldots, r_N]^T$$
$$\boldsymbol{S}(z) = [s_1, s_2, \ldots, s_N]^T \tag{16}$$

are the vectors of trial functions, whereas

$$\boldsymbol{q}_v(t) = \left[q_1^v, q_2^v, \ldots, q_N^v\right]^T, \qquad \boldsymbol{q}_R(t) = \left[q_1^R, q_2^R, \ldots, q_N^R\right]^T$$
$$\boldsymbol{q}_S(t) = \left[q_1^S, q_2^S, \ldots, q_N^S\right]^T \tag{17}$$

are vectors of generalized coordinates and the superscript T denotes the transpose operation of a matrix.

These representations of displacement measures are used directly in Hamilton's variational equation,

$$\delta J = \int_{t_0}^{t_1} (\delta T - \delta V + \delta W)\,\mathrm{d}t = 0 \tag{18}$$

which is considered in conjunctions with the conditions at $t = t_0, t_1$,

$$\delta v_0 = \delta\theta_x = \delta\Theta = 0 \tag{19}$$

In this context, the identity concerning the convolution integral

$$\int_{z_0}^{z_1} \delta_D^j(z - \zeta) g(z)\,\mathrm{d}z = (-1)^{(j)} g^j(\zeta) \tag{20}$$

which is valid when $\zeta \in [z_0,\ z_1]$, and where $Y''(z) = \delta_D'(z)$, $\delta_D(\ )$ being the spatial Dirac's distribution, and $\delta_D^j \equiv \mathrm{d}^j\delta_D/\mathrm{d}z^j$ will also be used.

Herein T and V are the kinetic and strain energies, respectively, W is the work done by the external distributed loads, t_0 and t_1 are two arbitrary instants of the time t, and δ is the variation operator.

Performing the integration with respect to the spanwise z coordinate and with respect to time, and keeping in mind Hamilton's condition, from Eq. (18) one obtains the discrete equations of motion:

$$\boldsymbol{M}\ddot{\boldsymbol{q}} + \boldsymbol{K}\boldsymbol{q} = \boldsymbol{Q} - \boldsymbol{F}\boldsymbol{u} \tag{21a}$$

where $\boldsymbol{M}$ and $\boldsymbol{K}$ are the mass and stiffness matrices, respectively, of the structure considered in its entirety, that is, of the host and piezoactuators, whereas $\boldsymbol{u}$ is the vector of the control input. In addition,

$$\boldsymbol{Q} = \int_0^L p_y v_i \, \mathrm{d}z \tag{21b}$$

$$\boldsymbol{F} = [r_i(z_2) - r_i(z_1)] \tag{21c}$$

are the generalized vector of time-dependent external excitations and the vector of piezoelectrically induced bending moment, respectively. These expression of $\boldsymbol{M}$ and $\boldsymbol{K}$ are displayed in Appendix A.

By the defining of the state vector as $\boldsymbol{x}(t) = [\boldsymbol{q}^T(t), \dot{\boldsymbol{q}}^T(t)]^T$ and then adding the identity $\dot{\boldsymbol{q}} = \dot{\boldsymbol{q}}$, Eq. (21a) can be cast in state-space form (e.g., see Ref. 7):

$$\dot{\boldsymbol{x}}(t) = \boldsymbol{A}\boldsymbol{x}(t) + \boldsymbol{B}\boldsymbol{Q}(t) + \boldsymbol{W}\boldsymbol{u}(t) \tag{22}$$

where

$$\boldsymbol{A} = \begin{bmatrix} \boldsymbol{0} & \boldsymbol{I} \\ -\boldsymbol{M}^{-1}\boldsymbol{K} & \boldsymbol{0} \end{bmatrix} \tag{23a}$$

$$\boldsymbol{B} = \begin{bmatrix} \boldsymbol{0} \\ \boldsymbol{M}^{-1} \end{bmatrix} \tag{23b}$$

$$\boldsymbol{W} = \begin{bmatrix} \boldsymbol{0} \\ -\boldsymbol{M}^{-1}\boldsymbol{F} \end{bmatrix} \tag{23c}$$

V. Optimal Feedback Control

For the optimal control problem, given an initial state $\boldsymbol{x}(t_0)$, the goal is to find a control vector $\boldsymbol{u}(t)$ defined on $t \in [t_0, \ t_f]$ that drives the state $\boldsymbol{x}(t_0)$ to the desired final state $\boldsymbol{x}(t_f)$ in such a way that a selected performance index is minimized. In a number of recent works (see Refs. 11–13), it was argued that the standard algorithms aimed at optimally controlling the structures exposed to time-dependent external excitations do not include the time-dependent external load in the performance index to be minimized. Incorporation of this term results in a time-dependent performance index that has to be minimized at any instant of time, where the terminology instantaneous optimal control afforded to this control algorithm comes from.

Upon adopting instantaneous optimal control concept and following the approach of Refs. 12 and 13, the augmented performance index including the constraint equation (22) is represented as

$$J_a(t) = \frac{1}{2}\boldsymbol{x}^T(t_f)\boldsymbol{T}\boldsymbol{x}(t_f) + \int_{t_0}^{t_f} \left\{ \frac{1}{2}(\boldsymbol{x}^T\boldsymbol{Z}\boldsymbol{x} + \boldsymbol{u}^T\boldsymbol{R}\boldsymbol{u}) + \boldsymbol{k}^T[\boldsymbol{A}\boldsymbol{x}(t) + \boldsymbol{W}\boldsymbol{u}(t) + \boldsymbol{B}\boldsymbol{Q}(t) - \dot{\boldsymbol{x}}] \right\} \mathrm{d}t \tag{24a}$$

in which $\boldsymbol{k}(t)$ is the vector of Lagrangian multipliers (referred to as the costates), $\boldsymbol{Z}$ and $\boldsymbol{R}$ are, respectively, positive semidefinite and positive weighting matrices, $\boldsymbol{T}$ is the nonnegative definite weighting matrix associated with the error in the terminal state at $t = t_f$, and $\boldsymbol{u}^T = [u_1, \ldots, u_m]$, where m is the number of piezoactuator patches. For large weighting matrix $\boldsymbol{Z}$, the response is small and the required active control $\boldsymbol{u}(t)$ will be large. As a result, suitable $\boldsymbol{Z}$ and $\boldsymbol{R}$ that provide a desired balance between the state variable responses and control efforts, while satisfying performance requirements and constraints, should be determined.

By expressing Eq. (24a) as

$$J_a(\boldsymbol{x}, \dot{\boldsymbol{x}}, \boldsymbol{k}; t) = \frac{1}{2}\boldsymbol{x}^T(t_f)\boldsymbol{T}\boldsymbol{x}(t_f) + \int_{t_0}^{t_f} g(\boldsymbol{x}, \dot{\boldsymbol{x}}, \boldsymbol{u}, \boldsymbol{k}; t) \, \mathrm{d}t \tag{24b}$$

where

$$g(\boldsymbol{x}, \dot{\boldsymbol{x}}, \boldsymbol{u}, \boldsymbol{k}; t) = \tfrac{1}{2}(\boldsymbol{x}^T\boldsymbol{Z}\boldsymbol{x} + \boldsymbol{u}^T\boldsymbol{R}\boldsymbol{u}) + \boldsymbol{k}^T[\boldsymbol{A}\boldsymbol{x}(t) + \boldsymbol{W}\boldsymbol{u}(t) + \boldsymbol{B}\boldsymbol{Q}(t) - \dot{\boldsymbol{x}}] \tag{24c}$$

the necessary conditions for the optimality can be found by setting the first variation of Eqs. (24) to be zero, which yields

$$\delta J_a = 0 = \delta\boldsymbol{x}^T(t_f)\boldsymbol{T}\boldsymbol{x}(t_f) + \int_{t_0}^{t_f} \left\{ \left(\frac{\partial g}{\partial \boldsymbol{x}}\right)^T \delta\boldsymbol{x} + \left(\frac{\partial g}{\partial \dot{\boldsymbol{x}}}\right)^T \delta\dot{\boldsymbol{x}} + \left(\frac{\partial g}{\partial \boldsymbol{u}}\right)^T \delta\boldsymbol{u} + \left(\frac{\partial g}{\partial \boldsymbol{k}}\right)^T \delta\boldsymbol{k} \right\} \mathrm{d}t \tag{25}$$

where

$$\frac{\partial g}{\partial \boldsymbol{x}} = \boldsymbol{Z}\boldsymbol{x} + \boldsymbol{A}^T\boldsymbol{k} \tag{26a}$$

$$\frac{\partial g}{\partial \dot{\boldsymbol{x}}} = -\boldsymbol{k} \tag{26b}$$

$$\frac{\partial g}{\partial \boldsymbol{u}} = \boldsymbol{R}\boldsymbol{u} + \boldsymbol{W}^T\boldsymbol{k} \tag{26c}$$

$$\frac{\partial g}{\partial \boldsymbol{k}} = \boldsymbol{A}\boldsymbol{x} + \boldsymbol{W}\boldsymbol{u} + \boldsymbol{B}\boldsymbol{Q} - \dot{\boldsymbol{x}} \tag{26d}$$

Integration by parts of the second term in Eq. (25) and making use of Eq. (26b) yields

$$\delta J_a = 0 = \int_{t_0}^{t_f} \left\{ \left[\frac{\partial g}{\partial \boldsymbol{x}} - \frac{\partial}{\partial t}\left(\frac{\partial g}{\partial \dot{\boldsymbol{x}}}\right)\right]\delta\boldsymbol{x} + \left(\frac{\partial g}{\partial \boldsymbol{u}}\right)^T \delta u + \left(\frac{\partial g}{\partial \boldsymbol{k}}\right)^T \delta\boldsymbol{k} \right\} \mathrm{d}t + \boldsymbol{k}^T(t_0)\delta\boldsymbol{x}(t_0) + \left[\boldsymbol{x}^T(t_f)\boldsymbol{T} - \boldsymbol{k}^T(t_f)\right]\delta\boldsymbol{x}(t_f) \tag{27}$$

In view of Eqs. (26) and (27), the necessary conditions for optimality are

$$\boldsymbol{Z}\boldsymbol{x} + \boldsymbol{A}^T\boldsymbol{k} + \dot{\boldsymbol{k}} = \boldsymbol{0} \tag{28a}$$

$$\boldsymbol{R}\boldsymbol{u} + \boldsymbol{W}^T\boldsymbol{k} = \boldsymbol{0} \tag{28b}$$

$$\dot{\boldsymbol{x}}(t) = \boldsymbol{A}\boldsymbol{x} + \boldsymbol{W}\boldsymbol{u} + \boldsymbol{B}\boldsymbol{Q} \tag{28c}$$

Because the initial conditions $\boldsymbol{x}(t_0)$ are known and the final states $\boldsymbol{x}(t_f)$ are assumed free, from Eq. (27) one obtain the boundary conditions

$$\delta\boldsymbol{x}(t_0) = \boldsymbol{0} \tag{29a}$$

which is equivalent to $\boldsymbol{x}(t_0) = \boldsymbol{x}_0$, and

$$\boldsymbol{x}^T(t_f)\boldsymbol{T} - \boldsymbol{k}^T(t_f) = \boldsymbol{0} \tag{29b}$$

To find the optimal feedback control law, we express Eqs. (28) as

$$\frac{\mathrm{d}}{\mathrm{d}t}\begin{bmatrix} \boldsymbol{x} \\ \boldsymbol{k} \end{bmatrix} = \begin{bmatrix} \boldsymbol{A} & -\boldsymbol{W}\boldsymbol{R}^{-1}\boldsymbol{W}^T \\ -\boldsymbol{Z} & -\boldsymbol{A}^T \end{bmatrix}\begin{bmatrix} \boldsymbol{x} \\ \boldsymbol{k} \end{bmatrix} + \begin{bmatrix} \boldsymbol{B}\boldsymbol{Q} \\ \boldsymbol{0} \end{bmatrix} \tag{30}$$

Denote $\boldsymbol{\Phi}$ as the transition matrix of the Eq. (30) and let it be partitioned according to the dimensions of $\boldsymbol{x}$ and $\boldsymbol{k}$ as follows:

$$\boldsymbol{\Phi} = \begin{bmatrix} \phi_{11} & \phi_{12} \\ \phi_{21} & \phi_{22} \end{bmatrix} \tag{31}$$

The solution of the Eq. (27) can be expressed in terms of final states as

$$\begin{bmatrix} \boldsymbol{x}(t) \\ \boldsymbol{k}(t) \end{bmatrix} = \begin{bmatrix} \phi_{11}(t - t_f) & \phi_{12}(t - t_f) \\ \phi_{21}(t - t_f) & \phi_{22}(t - t_f) \end{bmatrix}\begin{bmatrix} \boldsymbol{x}(t_f) \\ \boldsymbol{k}(t_f) \end{bmatrix} + \int_{t_f}^{t} \begin{bmatrix} \phi_{11}(t - \tau) & \phi_{12}(t - \tau) \\ \phi_{21}(t - \tau) & \phi_{22}(t - \tau) \end{bmatrix}\begin{bmatrix} \boldsymbol{B}\boldsymbol{Q} \\ \boldsymbol{0} \end{bmatrix} \mathrm{d}\tau \tag{32}$$

Using in Eq. (32) the boundary condition (29b), one obtains

$$\boldsymbol{x}(t) = \boldsymbol{\Phi}_{11}(t-t_f)\boldsymbol{x}(t_f) + \boldsymbol{\Phi}_{12}(t-t_f)\boldsymbol{T}\boldsymbol{x}(t_f) + \int_{t_f}^{t} \boldsymbol{\Phi}_{11}(t-\tau)\boldsymbol{B}\boldsymbol{Q}(\tau)\,\mathrm{d}\tau \tag{33a}$$

$$\boldsymbol{k}(t) = \boldsymbol{\Phi}_{21}(t-t_f)\boldsymbol{x}(t_f) + \boldsymbol{\Phi}_{22}(t-t_f)\boldsymbol{T}\boldsymbol{x}(t_f) + \int_{t_f}^{t} \boldsymbol{\Phi}_{21}(t-\tau)\boldsymbol{B}\boldsymbol{Q}(\tau)\,\mathrm{d}\tau \tag{33b}$$

Solving for $\boldsymbol{x}(t_f)$ from Eq. (33a) and then substituting it into Eq. (33b) yield the costates $\boldsymbol{k}(t)$

$$\boldsymbol{k}(t) = \boldsymbol{P}(t)\boldsymbol{x}(t) + \boldsymbol{d}(t) \tag{34}$$

where

$$\boldsymbol{P}(t) = [\boldsymbol{\Phi}_{21}(t-t_f) + \boldsymbol{\Phi}_{22}(t-t_f)\boldsymbol{T}][\boldsymbol{\Phi}_{11}(t-t_f) + \boldsymbol{\Phi}_{12}(t-t_f)\boldsymbol{T}]^{-1} \tag{35a}$$

and

$$\boldsymbol{d}(t) = -\boldsymbol{P}(t)\int_{t_f}^{t} \boldsymbol{\Phi}_{11}(t-\tau)\boldsymbol{B}\boldsymbol{Q}(\tau)\,\mathrm{d}\tau + \int_{t_f}^{t} \boldsymbol{\Phi}_{21}(t-\tau)\boldsymbol{B}\boldsymbol{Q}(\tau)\,\mathrm{d}\tau \tag{35b}$$

By virtue of Eqs. (28b) and (34), the linear optimal control law can be expressed as

$$\boldsymbol{u}(t) = -\boldsymbol{R}^{-1}\boldsymbol{W}^T\boldsymbol{P}(t)\boldsymbol{x}(t) - \boldsymbol{R}^{-1}\boldsymbol{W}^T\boldsymbol{d}(t) \tag{36}$$

To determine $\boldsymbol{P}(t)$ and $\boldsymbol{d}(t)$, we differentiate Eq. (34) with respect to time, which yields

$$\dot{\boldsymbol{k}} = \dot{\boldsymbol{P}}\boldsymbol{x} + \boldsymbol{P}\dot{\boldsymbol{x}} + \dot{\boldsymbol{d}} \tag{37a}$$

which by virtue of Eqs. (28) and (34) yields

$$\dot{\boldsymbol{k}} = -\boldsymbol{Z}\boldsymbol{x} - \boldsymbol{A}^T(\boldsymbol{P}\boldsymbol{x} + \boldsymbol{d}) \tag{37b}$$

$$\dot{\boldsymbol{x}} = \boldsymbol{A}\boldsymbol{x} - \boldsymbol{W}\boldsymbol{R}^{-1}\boldsymbol{W}^T\boldsymbol{k} + \boldsymbol{B}\boldsymbol{Q} \tag{37c}$$

Replacement of Eqs. (37b) and (37c) into (37a) and keeping in mind that the obtained equation holds for the states $\boldsymbol{x}(t)$, at any time $t \in [t_0, t_f]$, result in

$$\dot{\boldsymbol{P}} = -\boldsymbol{Z} - \boldsymbol{A}^T\boldsymbol{P} - \boldsymbol{P}\boldsymbol{A} + \boldsymbol{P}\boldsymbol{W}\boldsymbol{R}^{-1}\boldsymbol{W}^T\boldsymbol{P} \tag{38a}$$

$$\dot{\boldsymbol{d}} = -(\boldsymbol{A}^T - \boldsymbol{P}\boldsymbol{W}\boldsymbol{R}^{-1}\boldsymbol{W}^T)\boldsymbol{d} - \boldsymbol{P}\boldsymbol{B}\boldsymbol{Q} \tag{38b}$$

To determine $\boldsymbol{P}(t)$ and $\boldsymbol{d}(t)$, which appear in the optimal control law described by Eq. (36), the preceding two equations have to be integrated backward in time in conjunction with the conditions at $t = t_f$:

$$\boldsymbol{P}(t_f) = \boldsymbol{T} \tag{39a}$$

$$\boldsymbol{d}(t_f) = \boldsymbol{0} \tag{39b}$$

When $\boldsymbol{B}\boldsymbol{Q}$ is neglected in the functional $J_a(t)$, by virtue of Eq. (35b), yielding $\boldsymbol{d} = 0$, a simplification of the optimal control law is emerging.

If, in addition, the terminal time t_f approaches infinity, the Riccati gain matrix $\boldsymbol{P}(t)$ becomes a constant matrix P_c, which is the solution to the nonlinear algebraic Riccati equation

$$\boldsymbol{A}^T\boldsymbol{P}_c + \boldsymbol{P}_c\boldsymbol{A} - \boldsymbol{P}_c\boldsymbol{W}R^{-1}\boldsymbol{W}^T\boldsymbol{P}_c + \boldsymbol{Z} = \boldsymbol{0} \tag{40}$$

obtained as a special case of Eqs. (38a). In this case, the corresponding steady-state linear optimal control law is given by

$$\boldsymbol{u}(t) = -\boldsymbol{G}^T\boldsymbol{x}(t) \tag{41}$$

where the optimal gain matrix in the steady-state case is given by

$$\boldsymbol{G} = \boldsymbol{R}^{-1}\boldsymbol{W}^T\boldsymbol{P} \tag{42}$$

Under a number of conditions, the algebraic Riccati equation has a unique, positive definite solution $\boldsymbol{P}_c$ that minimizes the performance index

$$J = \frac{1}{2}\int_0^{\infty} [\boldsymbol{x}^T\boldsymbol{Z}\boldsymbol{x} + \boldsymbol{u}^T\boldsymbol{R}\boldsymbol{u}]\,\mathrm{d}t \tag{43}$$

when the control law, Eq. (41), in conjunction with Eq. (42) is used.

Note that the state weighting matrix $\boldsymbol{Z}$ was chosen so that the first term in the cost functional represents the sum of the system kinetic and potential energies

$$\frac{1}{2}\int_0^{\infty} [\boldsymbol{x}^T\boldsymbol{Z}\boldsymbol{x}]\,\mathrm{d}t = \frac{1}{2}\int_0^{\infty} [\dot{\boldsymbol{q}}^T\boldsymbol{M}\dot{\boldsymbol{q}} + \boldsymbol{q}^T\boldsymbol{K}\boldsymbol{q}]\,\mathrm{d}t \tag{44}$$

where $\boldsymbol{q}$ are vectors of generalized coordinates.

Furthermore, $\boldsymbol{R}$ was chosen as $\boldsymbol{R} = \alpha\boldsymbol{F}^T\boldsymbol{K}\boldsymbol{F}$ (see Ref. 14) from the consideration of the structural configuration as well as actuator location, where $\boldsymbol{F}$ represents actuator influence vector $r_i'(z)$ and α is a scaling factor. This enables one to synthesize the controllers to achieve a proper tradeoff between control effectiveness and control energy consumption by varying the relative magnitudes of $\boldsymbol{Z}$ and $\boldsymbol{R}$. However, by virtue of Eq. (44), only $\boldsymbol{R}$ remains as the design parameter.

As mentioned, in the case of piezoactuators spread over the entire span of the beam, the piezoelectrically induced bending moment $\hat{M}_x$ appears in the boundary condition at $z = L$, only. Its expression is

$$\hat{M}_x = \boldsymbol{F}u, \qquad u = \mathcal{C}V(t) \tag{45a}$$

$$\boldsymbol{F} = r_i'(L) \tag{45b}$$

In addition to this modification, the mass and the stiffness are obtained by setting $\delta_P = 0$ and $\delta_S = 1$ in Eqs. (13).

VI. Saturation Constraint

In some situations, the required control moment can exceed the moment output capability provided by the actuator. This is due to the limited voltage that can be applied to the piezoactuator. Beyond this limited value, the saturation of the piezoactuator occurs. There are several approaches enabling one to handle the problem of the optimal control subjected to saturation constraint of the controller. Within this study, the idea presented in Refs. 15 and 16 enabling implementation of the optimal control in both unsaturated and saturated regions of the actuator will be followed. In this case, rather than reducing the feedback gains to accommodate the constraint, the actuator limitation is explicitly addressed in the optimal control algorithm. To reflect the control force limitation on the actuator, the commanded control output must satisfy for $t \in [t_0, t_\infty]$ the condition

$$-u_{\max} \le u(t) \le u_{\max} \tag{46}$$

For the unsaturated controller, the optimal controller is obtained as

$$\boldsymbol{u}(t) = -\boldsymbol{R}^{-1}\boldsymbol{W}^T\boldsymbol{k}(t) \tag{47}$$

In light of Eq. (46), this is valid for

$$|-\boldsymbol{R}^{-1}\boldsymbol{W}^T\boldsymbol{k}(t)| \le u_{\max} \tag{48}$$

VII. Sensor Output Equation: Power Required for the Control

Herein one assumes that the piezoelectric elements can be employed concurrently for sensing and actuation. For the sensing operation, setting $\mathcal{E}_3 = 0$, the electric displacement results as

$$D_3 = e_{31}S_{zz} \tag{49}$$

and keeping in view the expression of the strain measure in the piezofilm, one obtains

$$D_3 = -e_{31}y(s)\theta_x' \tag{50}$$

The electric charge due to the direct effect of the PZT materials can be found through integration of the electric displacement over the corresponding sensor area, so that

$$q_p(t) = \int_A D_3 \, dA = -\int\int e_{31} y(s) \theta_x' \, ds \, dz \tag{51}$$

The limits of integration in Eq. (51) depend on the sensor-patch configuration.

The voltage across the piezoelectric sensor can be found by dividing the charge developed in the sensor by the sensor's capacitance C_p (see Ref. 17),

$$V_p(t) = q_p(t)/C_p \tag{52}$$

where C_p depends on the patch area A_p, thickness h^a, and the permittivity of the piezoelectric material ξ_{33}^p, according to (see Ref. 18)

$$C_p = \xi_{33}^p A_p \Big| \; h^a \tag{53}$$

The electric current required for vibration suppression is

$$I = \frac{dq_p(t)}{dt} = -\int e_{31} y(s) \dot{\theta}_x' \, ds \, dz$$

$$= -\int e_{31} y(s) [\dot{\theta}_x(z_2) - \dot{\theta}_x(z_1)] \, ds \tag{54}$$

Accordingly, the electric power consumption can be obtained as the product of the applied control voltage and current as $P = VI$.

VIII. Time-Dependent Loads Associated with Blast and Sonic-Boom Pulses

The case of explosive blast and sonic-boom overpressure signatures will be considered. As was clearly established, the blast wave reaches the peak value in such a short time that the structure can be assumed to be loaded instantly and uniformly in the spanwise direction. In Appendix B the pressure pulses used in the present study are recorded. In addition, diagrammatic representations of considered pressure pulses are included as insets in Figs. 2 through 12.

IX. Numerical Illustrations and Discussion

Although the obtained results are valid for an arbitrary cross-sectional beam shape, the displayed numerical results are restricted to the case of a cantilevered thin-walled beam of symmetric biconvex cross section profile proper to a high-speed wing aircraft (see Fig. 1a where its geometric characteristics are shown). For the material of the host structure, two cases are considered in the numerical applications: 1) a graphite–epoxy composite with its on-axis elastic properties provided in Refs. 3–6 and 2) a transversely isotropic material characterized by the Young's modulus E in the surface of isotropy (coinciding with the beam midsurface) and the transverse shear modulus G' in the planes normal to the isotropy surfaces. The piezopatch manufactured of PZT-4 piezoceramic (for its properties see Refs. 6 and 7) is located as indicated in Fig. 1b. Throughout these results, $P_m = 50$ lb/L, and the aspect ratio of the beam, unless otherwise specified, is $AR(\equiv 2L/c) = 6$. In addition, the mass density of the material considered is $\rho = 0.70135 \times 10^{-3}$ lb·s^2/in. for the transversely isotropic materials (Figs. 2–4), and $\rho = 0.143 \times 10^{-3}$ lb·s^2/in. for the graphite–epoxy material (Figs. 5–12). In Fig. 2, the controlled/uncontrolled time-history of the beam tip dimensionless transversal deflection $\tilde{V}(\equiv v_0/L)$ of a transversely isotropic beam subjected to a triangular-blast pulse, for selected locations along the beam span of the piezopatch actuator of fixed size ($z^a = 0.1L$) is shown.

The results reveal that from the point of view of the control efficiency the best location of the piezopatch actuator is that toward the beam root. The results emerging from Fig. 2 reveal that the control efficiency decays as piezopatch location shifts toward the beam tip. A similar conclusion was obtained in another context in Ref. 19.

In Fig. 3, the effect of transverse shear flexibility on dimensionless beam tip transverse deflection time history of the controlled and uncontrolled structure exposed to a sonic boom is shown. The results show that for the uncontrolled structure, the unshearable beam model, that is, corresponding to $E/G' = 0$ underestimates the transverse deflection as predicted by the shearable structure, that is, characterized by $E/G' = 100$, in both the forced and free motion regimes, a trend which is exacerbated in the latter motion regime.

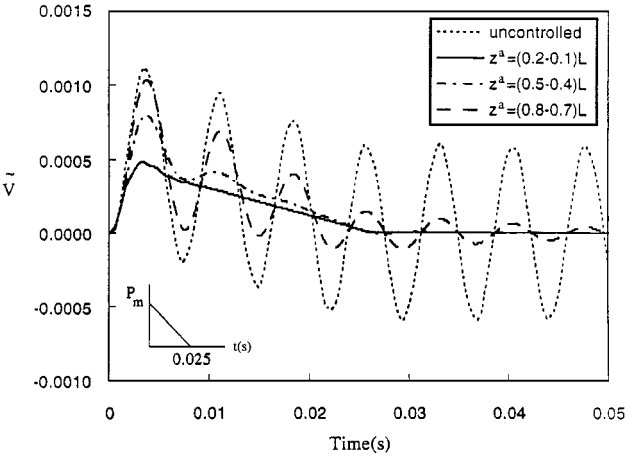

Fig. 2 Influence of the piezopatch location on beam dimensionless tip deflection time history; $E/G' = 100$ and $P_m = 50$ lb/L. The case of the unactivated beam is also displayed; blast loading.

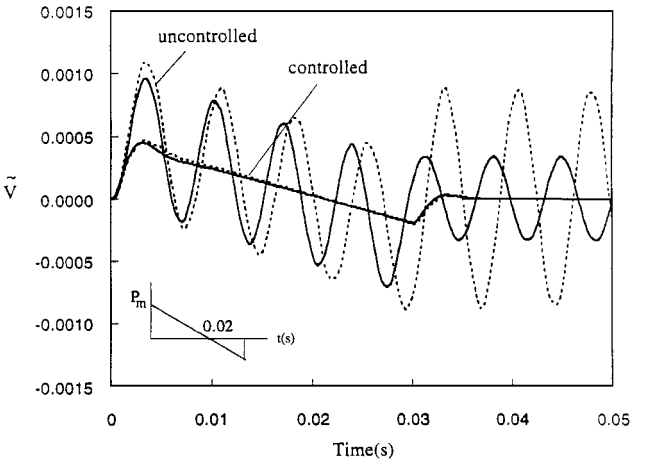

Fig. 3 Influence of transverse shear on beam dimensionless tip deflection time history. The beam is exposed to a sonic-boom wave ($t_p = 0.002$ s and $r = 2.5$: ——, $E/G' = 0$, and ····, $E/G' = 100$).

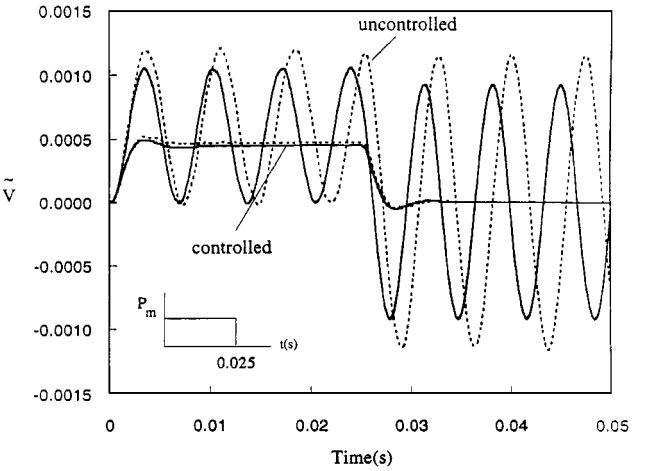

Fig. 4 Influence of transverse shear on beam dimensionless tip deflection time history: ——, $E/G' = 0$, and ····, $E/G' = 100$; rectangular pulse.

On the other hand, for the controlled beam, the differences of the response deflections obtained for shearable and unshearable beams, in both free and forced motion ranges, are hardly detectable.

Similar but not identical conclusions also emerge in the case of a rectangular pressure pulse (Fig. 4). Note from Fig. 4, in this case, the

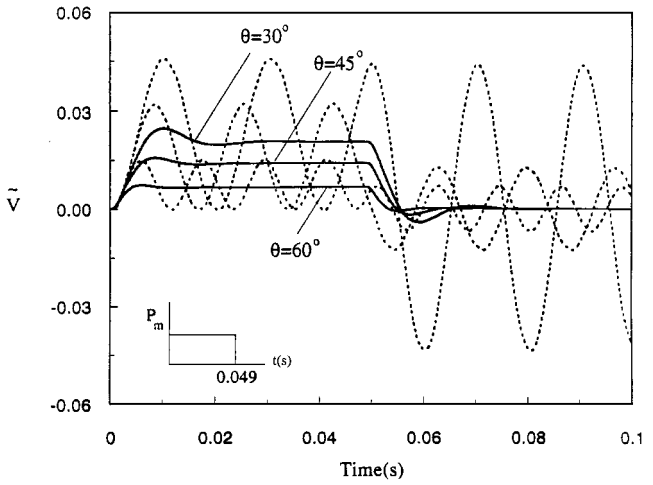

Fig. 5 Influence of the ply-angle orientation on beam dimensionless tip deflection time history. Unshearable and free warping beam model; rectangular pulse. The patch extension is $z_a = (0.2\text{–}0.1)L$: ——, activated structure, and ···, unactivated structure.

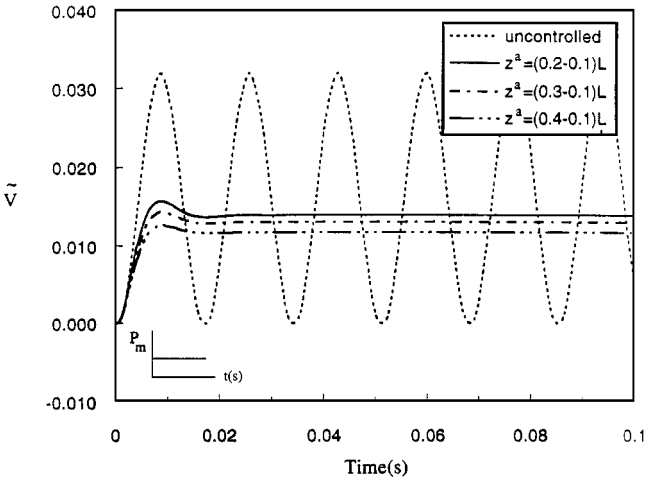

Fig. 6 Influence of the piezopatch size on the beam time-history dimensionless tip deflection; unshearable and free warping beam model, $\theta = 45$ deg, and step pulse.

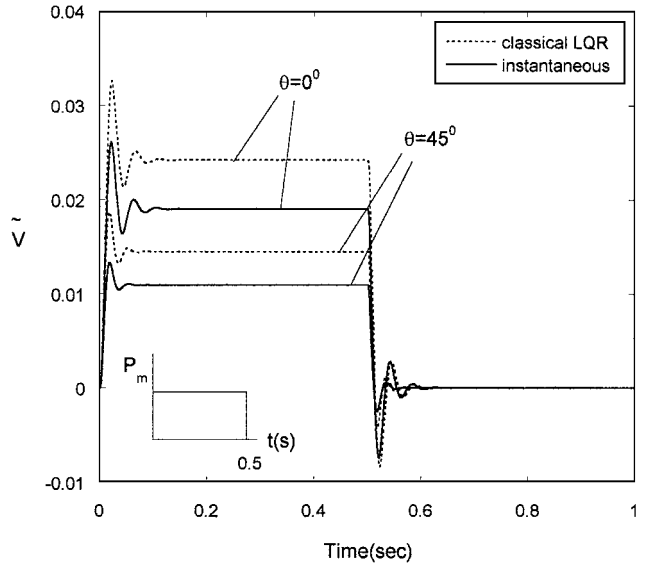

Fig. 7 Influence on the transversal deflection time history of the discard (···, classical optimal control) and incorporation of the external excitation (——, instantaneous optimal control) in the performance index, coupled with that of the ply-angle distribution ($\theta = 0$ and 45 deg). Unshearable and free warping beam model; rectangular pulse, L = 30 in. (0.76 m); $z^a = (0.2\text{–}0.1)\,L$.

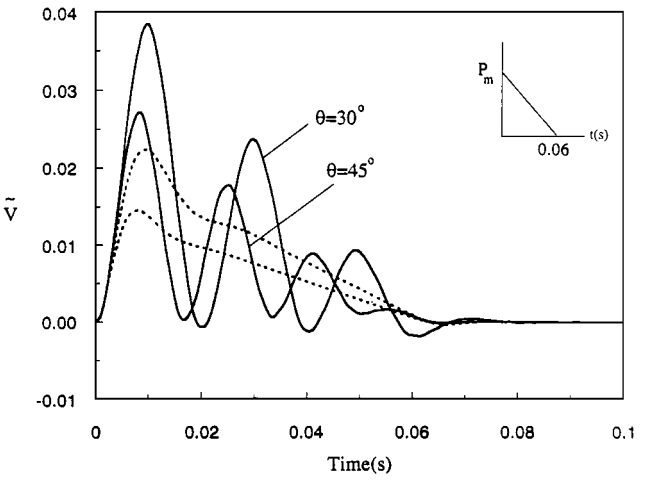

Fig. 8 Influence of the voltage control constraint considered in conjunction with the ply-angle orientation of the beam material on dimensionless tip deflection time history. Unshearable and free warping beam model: ——, $V_{\max} = 250$ V, and ···, unlimited voltage; blast pulse.

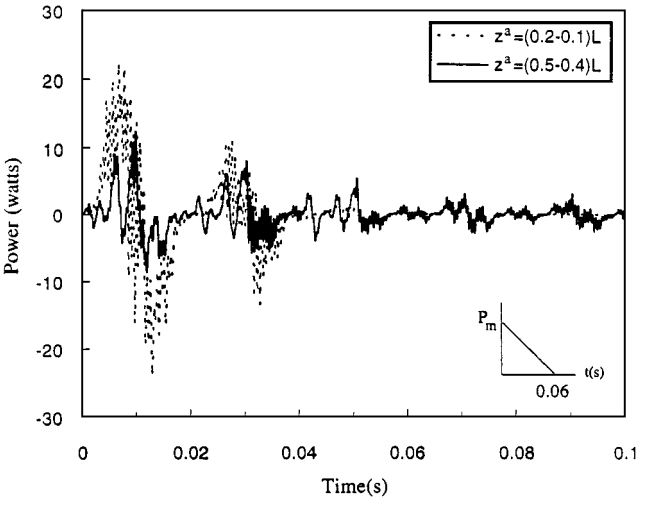

Fig. 9 Influence of the location of the piezopatch on the required electric power. Unshearable and free warping beam model, ply-angle θ = 30 deg, constrained voltage (= 250 V), blast pulse.

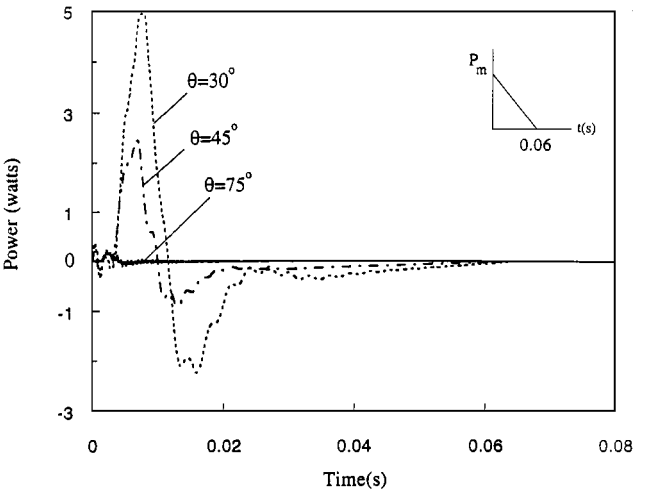

Fig. 10 Influence of the ply-angle orientation on the required electric power. Unshearable and free warping beam model; $z^a = (0.2\text{–}0.1)L$; unconstrained voltage, blast pulse.

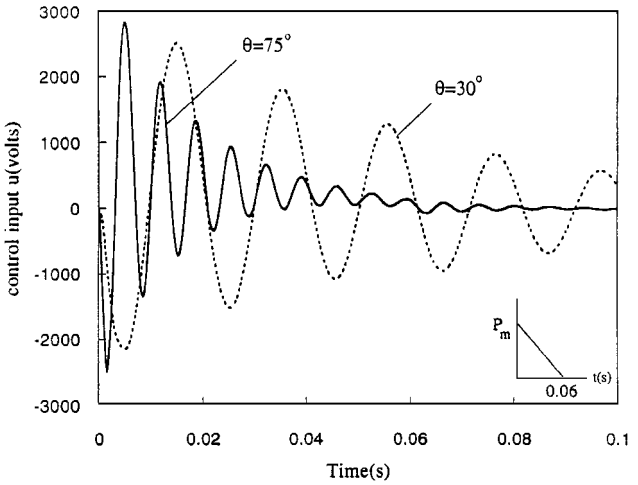

Fig. 11 Influence of ply-angle orientation on control input voltage time history; no input voltage limitations, piezopatch is located at $z^a = (0.8–0.7)L$; unshearable and free warping beam model; blast pulse.

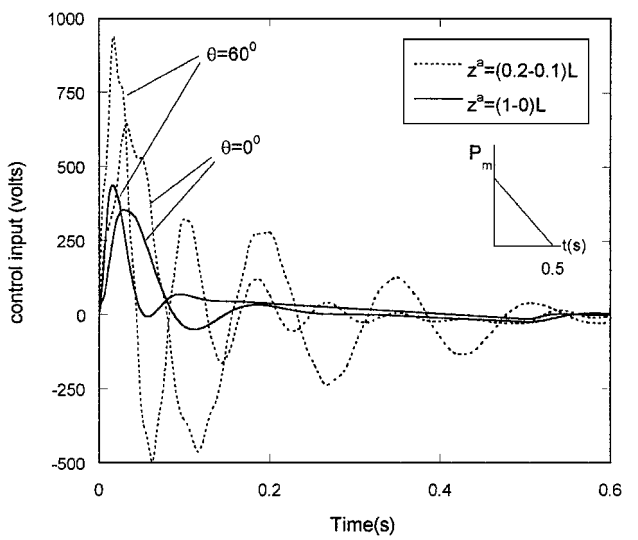

Fig. 12 Influence of the actuator size and of ply angle on the control input voltage. Unshearable and free warping beam model; instantaneous optimal control, blast pulse ($\bar{R}$ = 16).

differences for the transverse deflection time history of shearable and unshearable beams in the free and forced motion regimes appear less pronounced as compared to those emerging in the case illustrated in Fig. 3.

In Fig. 5, the effect of the ply-angle orientation on transverse beam dimensionless tip deflection time history of the activated and nonactivated structure exposed to a rectangular pressure pulse is highlighted. The results reveal that, with the increase of the ply angle, which is associated with an increase of the flexural stiffness (see Ref. 5), a strong confinement of the deflection increase in the forced motion regime, for both the activated and unactivated structure, is obtained.

This trend also remains valid in the free motion regime for the unactivated beam, whereas for the activated beam, in view of the high efficiency of the feedback control, the influence of the tailoring becomes almost immaterial.

The effect of the size of the piezoactuator on the transversal tip beam deflection time history is recorded in Fig. 6. The results reveal that when the location of the piezopatch actuator is close to the beam root, the control efficiency is almost identical to that of the piezoactuator featuring larger sizes.

In Fig. 7, the comparison between the results emerging in the case of the instantaneous control and classical optimal control methodologies for two ply-angle configurations is displayed. The results reveal that, especially in the forced motion range, nonnegligible differences in the deflection response occur when the external excitation is discarded in the performance index, as compared to the more exact perdictions obtained when the external excitations are included in the performance index. The obtained results also reveal that: 1) the classical linear quadratic regulator (LQR) control overpredicts the deflection amplitude in the forced motion regime as compared to that predicted by the instantaneous LQR, and 2) the increase of the ply angle yields a containment of the deflection increase. The obtained results, not displayed here, reveal that the elastic twist is also strongly influenced by the increase of the ply angle, in the same sense as the transverse deflection.

In the preceding numerical examples no limitation on the control input voltage $V(t)$ was imposed. However, in realistic problems, the depoling voltage of 250 V in the current actuator configuration should be considered as a limitation of the piezoactuators. In Fig. 8, the solid lines correspond to limited voltage, $V_{\max} = \pm 250$ V, whereas the dotted lines correspond to the case when no limitation on the voltage was imposed. The results reveal that even in the case of the constrained voltage, implementation of a ply angle resulting in an increase of the flexural stiffness can yield an enhanced dynamic response within the forced motion regime.

Related with the power consumption, location of the piezoactuator has a significant influence on the power requirements during the suppression of the beam vibration. It is found that when the piezoactuator is located toward the root of the beam, that is, when control effectiveness increases, the power consumption of the piezoactuator increases as well. Such a result was also reported in Ref. 19. In Fig. 9, the time history of the power consumption for two cases of the patch location is displayed. The maximum power demand for the piezoactuator location $z^a = (0.5–0.4)L$ is approximately 33% of the peak value corresponding to the location $z^a = (0.2–0.1)L$.

In Fig. 10 the effect of ply-angle orientation on electrical power consumption is shown. The results reveal that with the increase of the ply angle, yielding an increase of the flexural stiffness of the beam, a decay in the electrical power consumption is experienced. The results not displayed here revealed that the same trend occurs when a constraint in the amplitude control voltage is imposed.

Time-history input control voltage applied to PZT actuators is recorded in Fig. 11 for the case of unconstrained control voltage. The results emerging from Fig. 11 reveal that the increase of the ply-angle that is accompanied by an increase of the beam stiffnesses, results in an augmentation of the *maximum* control input voltage. At the same time, results not displayed here reveal that, as compared to the beam model incorporating warping inhibition, the free warping model yields a slight increase of the control input voltage.

The influence played by the size of piezoactuators in conjuction with that of the ply angle of the material of the host structure on the control input voltage time history is recorded in Fig. 12. The results reveal that within the forced motion regime, a lower control input voltage is needed in the case of the piezoactuator spread over the entire span of the beam than in the case of a piezopatch. In addition, from Fig. 12 it becomes evident that an increase of the stiffness of the structure induced by an increase of the ply angle is accompanied by an increase of the control input voltage, especially in the forced motion regime.

X. Conclusions

A number of issues related with the influence of nonclassical effects on the optimal feedback control of the dynamic response of thin-walled beams subjected to blast pulses have been investigated. Among others, issues related with the influence of the location and size of piezoelectric patches, optimal control with input voltage constraint, input power consumption, and effects resulting from the inclusion in the performance index of external excitations have been explored. The presented results reveal the synergistic interaction and efficiency emerging from the implemented control methodology based on the simultaneous application of the optimal feedback control and of the tailoring technique, on the dynamic response of cantilevered thin-walled beams exposed to time-dependent external excitations.

Appendix A: Matrices M and K Corresponding to a Number of Special Cases

The first is the case of the beam whose material is transversely isotropic, the plane of isotropy coinciding at each point to the beam midsurface. In this case, the bending and twist become decoupled. Herein the bending is considered only. Corresponding to this case we have

$$\boldsymbol{M} = \int_0^L \begin{bmatrix} (\bar{b}_1 + \delta_S \hat{\bar{b}}_1)\boldsymbol{V}\boldsymbol{V}^T & 0 \\ 0 & (\bar{b}_2 + \delta_S \hat{\bar{b}}_2)\boldsymbol{S}\boldsymbol{S}^T \end{bmatrix} \mathrm{d}z + \delta_P \int_{z_1}^{z_2} \begin{bmatrix} \hat{b}_1 \boldsymbol{V}\boldsymbol{V}^T & 0 \\ 0 & \hat{b}_2 \boldsymbol{S}\boldsymbol{S}^T \end{bmatrix} \mathrm{d}z \tag{A1}$$

$$\boldsymbol{K} = \int_0^L \begin{bmatrix} (\bar{a}_{55} + \delta_S \hat{\bar{a}}_{55})\boldsymbol{V}'\boldsymbol{V}'^T & (\bar{a}_{55} + \delta_S \hat{\bar{a}}_{55})\boldsymbol{V}'\boldsymbol{R}^T \\ (\bar{a}_{55} + \delta_S \hat{\bar{a}}_{55})\boldsymbol{R}\boldsymbol{V}'^T & (a_{55} + \delta_S \hat{\bar{a}}_{55})\boldsymbol{R}\boldsymbol{R}^T + (a_{33} + \delta_S \hat{\bar{a}}_{33})\boldsymbol{R}'\boldsymbol{R}'^T \end{bmatrix} \mathrm{d}z + \delta_P \int_{z_1}^{z_2} \begin{bmatrix} \hat{a}_{55}\boldsymbol{V}'\boldsymbol{V}'^T & \hat{a}_{55}\boldsymbol{V}'\boldsymbol{R}^T \\ \hat{a}_{55}\boldsymbol{R}\boldsymbol{V}'^T & \hat{a}_{55}\boldsymbol{R}\boldsymbol{R}^T + \hat{a}_{33}\boldsymbol{R}'\boldsymbol{R}'^T \end{bmatrix} \mathrm{d}z \tag{A2}$$

Second is the case of the unshearable host structure incorporating warping inhibition and manufactured of an anisotropic material (CAS ply-angle configuration). For this case, $\boldsymbol{M}$ is given by Eq. (A1) and

$$\boldsymbol{K} = \int_0^L \begin{bmatrix} (\bar{a}_{33} + \delta_S \hat{\bar{a}}_{55})\boldsymbol{V}''\boldsymbol{V}''^T & -(\bar{a}_{37} + \delta_S \hat{\bar{a}}_{37})\boldsymbol{V}''\boldsymbol{S}'^T \\ -(\bar{a}_{37} + \delta_S \hat{\bar{a}}_{37})\boldsymbol{S}'\boldsymbol{V}''^T & -(\bar{a}_{66} + \delta_S \hat{\bar{a}}_{66})\boldsymbol{S}'\boldsymbol{S}'''^T + (\bar{a}_{77} + \delta_S \hat{\bar{a}}_{77})\boldsymbol{S}'\boldsymbol{S}'^T \end{bmatrix} \mathrm{d}z + \delta_P \int_{z_1}^{z_2} \begin{bmatrix} \hat{a}_{33}\boldsymbol{V}''\boldsymbol{V}''^T & -\hat{a}_{37}\boldsymbol{V}''\boldsymbol{S}'^T \\ -\hat{a}_{37}\boldsymbol{S}'\boldsymbol{V}''^T & -\hat{a}_{66}\boldsymbol{S}'\boldsymbol{S}'''^T + \hat{a}_{77}\boldsymbol{S}'\boldsymbol{S}'^T \end{bmatrix} \mathrm{d}z \tag{A3}$$

Third is the case of shearable host structure featuring free warping and manufactured of an anisotropic material (ply-angle configuration provided by Eq. 5). In this case,

$$\boldsymbol{M} = \int_0^L \begin{bmatrix} (\bar{b}_1 + \delta_S \hat{\bar{b}}_1)\boldsymbol{V}\boldsymbol{V}^T & 0 & 0 \\ 0 & (\bar{b}_2 + \delta_S \hat{\bar{b}}_2)\boldsymbol{R}\boldsymbol{R}^T & 0 \\ 0 & 0 & (\bar{b}_3 + \delta_S \hat{\bar{b}}_3)\boldsymbol{S}\boldsymbol{S}^T \end{bmatrix} \mathrm{d}z + \delta_P \int_{z_1}^{z_2} \begin{bmatrix} \hat{b}_1 \boldsymbol{V}\boldsymbol{V}^T & 0 & 0 \\ 0 & \hat{b}_2 \boldsymbol{R}\boldsymbol{R}^T & 0 \\ 0 & 0 & \hat{b}_3 \boldsymbol{S}\boldsymbol{S}^T \end{bmatrix} \mathrm{d}z \tag{A4}$$

$$\boldsymbol{K} = \int_0^L \begin{bmatrix} (\bar{a}_{55} + \delta_S \hat{\bar{a}}_{55})\boldsymbol{V}'\boldsymbol{V}'^T & (\bar{a}_{55} + \delta_S \hat{\bar{a}}_{55})\boldsymbol{V}'\boldsymbol{R}^T & 0 \\ (\bar{a}_{55} + \delta_S \hat{\bar{a}}_{55})\boldsymbol{R}\boldsymbol{V}'^T & (\bar{a}_{55} + \delta_S \hat{\bar{a}}_{55})\boldsymbol{R}\boldsymbol{R}^T + (\bar{a}_{33} + \delta_S \hat{\bar{a}}_{33})\boldsymbol{R}'\boldsymbol{R}'^T & (\bar{a}_{37} + \delta_S \hat{\bar{a}}_{37})\boldsymbol{R}'\boldsymbol{S}'^T \\ 0 & (\bar{a}_{37} + \delta_S \hat{\bar{a}}_{37})\boldsymbol{S}'\boldsymbol{R}'^T & (\bar{a}_{77} + \delta_S \hat{\bar{a}}_{77})\boldsymbol{S}'\boldsymbol{S}'^T \end{bmatrix} \mathrm{d}z$$

$$+ \delta_P \int_{z_1}^{z_2} \begin{bmatrix} \hat{a}_{55}\boldsymbol{V}'\boldsymbol{V}'^T & \hat{a}_{55}\boldsymbol{V}'\boldsymbol{R}^T & 0 \\ \hat{a}_{55}\boldsymbol{R}\boldsymbol{V}'^T & \hat{a}_{55}\boldsymbol{R}\boldsymbol{R}^T + \hat{a}_{33}\boldsymbol{R}'\boldsymbol{R}'^T & \hat{a}_{37}\boldsymbol{R}'\boldsymbol{S}'^T \\ 0 & \hat{a}_{37}\boldsymbol{S}'\boldsymbol{R}'^T & \hat{a}_{77}\boldsymbol{S}'\boldsymbol{S}'^T \end{bmatrix} \mathrm{d}z \tag{A5}$$

Fourth is the case of shearable host structure incorporating warping inhibition, its material featuring anisotropic properties (ply-angle configuration provided by Eq. 5). $\boldsymbol{M}$ is given by Eq. (A4) and

$$\boldsymbol{K} = \int_0^L \begin{bmatrix} (\bar{a}_{55} + \delta_S \hat{\bar{a}}_{55})\boldsymbol{V}'\boldsymbol{V}'^T & (\bar{a}_{55} + \delta_S \hat{\bar{a}}_{55})\boldsymbol{V}'\boldsymbol{R}^T & (\bar{a}_{56} + \delta_S \hat{\bar{a}}_{56})\boldsymbol{V}'\boldsymbol{S}''^T \\ (\bar{a}_{55} + \delta_S \hat{\bar{a}}_{55})\boldsymbol{R}\boldsymbol{V}'^T & (\bar{a}_{55} + \delta_S \hat{\bar{a}}_{55})\boldsymbol{R}\boldsymbol{R}^T + (\bar{a}_{33} + \delta_S \hat{\bar{a}}_{33})\boldsymbol{R}'\boldsymbol{R}'^T & (\bar{a}_{37} + \delta_S \hat{\bar{a}}_{37})\boldsymbol{R}'\boldsymbol{S}'^T + (\bar{a}_{56} + \delta_S \hat{\bar{a}}_{56})\boldsymbol{S}''\boldsymbol{R}^T \\ (\bar{a}_{56} + \delta_S \hat{\bar{a}}_{56})\boldsymbol{S}''\boldsymbol{V}'^T & (\bar{a}_{37} + \delta_S \hat{\bar{a}}_{37})\boldsymbol{S}'\boldsymbol{R}'^T + (\bar{a}_{56} + \delta_S \hat{\bar{a}}_{56})\boldsymbol{S}''\boldsymbol{R}^T & (\bar{a}_{77} + \delta_S \hat{\bar{a}}_{77})\boldsymbol{S}'\boldsymbol{S}'^T + (\bar{a}_{66} + \delta_S \hat{\bar{a}}_{66})\boldsymbol{S}''\boldsymbol{S}''^T \end{bmatrix} \mathrm{d}z$$

$$+ \delta_P \int_{z_1}^{z_2} \begin{bmatrix} \hat{a}_{55}\boldsymbol{V}'\boldsymbol{V}'^T & \hat{a}_{55}\boldsymbol{V}'\boldsymbol{R}^T & \hat{a}_{56}\boldsymbol{V}'\boldsymbol{S}''^T \\ \hat{a}_{55}\boldsymbol{R}\boldsymbol{V}'^T & \hat{a}_{55}\boldsymbol{R}\boldsymbol{R}^T + \hat{a}_{33}\boldsymbol{R}'\boldsymbol{R}'^T & \hat{a}_{37}\boldsymbol{R}'\boldsymbol{S}'^T + \hat{a}_{56}\boldsymbol{S}''\boldsymbol{R}^T \\ \hat{a}_{56}\boldsymbol{S}''\boldsymbol{V}'^T & \hat{a}_{37}\boldsymbol{S}'\boldsymbol{R}'^T + \hat{a}_{56}\boldsymbol{S}''\boldsymbol{R}^T & \hat{a}_{77}\boldsymbol{S}'\boldsymbol{S}'^T + \hat{a}_{66}\boldsymbol{S}''\boldsymbol{S}''^T \end{bmatrix} \mathrm{d}z \tag{A6}$$

Last is the case of an unshearable host structure featuring free twist, whose material exhibits anisotropic properties (ply-angle configuration provided by Eq. 5). $\boldsymbol{M}$ is given by Eq. (A1), and

$$\boldsymbol{K} = \int_0^L \begin{bmatrix} (\bar{a}_{33} + \delta_S \hat{\bar{a}}_{33})\boldsymbol{V}''\boldsymbol{V}''^T & -(\bar{a}_{37} + \delta_S \hat{\bar{a}}_{37})\boldsymbol{V}''\boldsymbol{S}'^T \\ -(\bar{a}_{37} + \delta_S \hat{\bar{a}}_{37})\boldsymbol{S}'\boldsymbol{V}''^T & (\bar{a}_{77} + \delta_S \hat{\bar{a}}_{77})\boldsymbol{S}'\boldsymbol{S}'^T \end{bmatrix} \mathrm{d}z + \delta_P \int_{z_1}^{z_2} \begin{bmatrix} \hat{a}_{33}\boldsymbol{V}''\boldsymbol{V}''^T & -\hat{a}_{37}\boldsymbol{V}''\boldsymbol{S}'^T \\ -\hat{a}_{37}\boldsymbol{S}'\boldsymbol{V}''^T & \hat{a}_{77}\boldsymbol{S}'\boldsymbol{S}'^T \end{bmatrix} \mathrm{d}z \tag{A7}$$

Appendix B: Time-Dependent Pressure Pulses

1) The overpressure associated with the blast pulses can be described in terms of the modified Friedlander exponential decay equation as (see Refs. 20 and 21),

$$p_y(s, z, t)[\equiv p_y(t)] = P_m(1 - t/t_p)e^{-a't/t_p} \tag{B1}$$

where the negative phase of the blast is included. In Eq. (B1), P_m is the peak reflected pressure in excess of the ambient one; t_p is the positive phase duration of the pulse measured from the time of impact of the structure, and a' is a decay parameter that has to be adjusted to approximate the overpressure signature from the blast tests. The ratio p_y/P_m vs. time for various blast signatures are shown

in the insets of figures where the control to these loads is concerned. As may be inferred, the triangular pulse may be viewed as a limiting case of Eq. (B2), occurring for $a'/t_p \to 0$.

2) The sonic-boom wave signature can be modeled as an N-shaped pressure pulse arriving at a normal incidence. Such a pulse corresonds to an idealized far-field overpressure produced by an aircraft flying supersonically in the Earth's atmosphere or by any supersonic projectile rocket or missile. The overpressure signature of the N-wave shock pulse can be described by (see Refs. 20 and 21)

$$p_y(s, z, t)[\equiv p_y(t)] = \begin{cases} P_m(1 - t/t_p) & \text{for} \quad 0 < t < rt_p \\ 0 & \text{for} \quad t > rt_p \end{cases} \tag{B2}$$

where r is the shock pulse length factor and P_m and t_p maintain the same meaning as in the case of blast pulses.

3) The step pressure pulse can be viewed as a special case of blast and sonic-boom pulses. This case is obtained either from Eq. (B1), when $t_p \to \infty$, or from Eq. (B2) when $r = 1$ and $t_p \to \infty$.

4) The case of the rectangular pressure pulse

$$p_y(s, z, t)[(\equiv p_y(t)] = \begin{cases} P_m & 0 \le t \le t_p \\ 0 & t > t_p \end{cases} \tag{B3}$$

will also be considered in this study.

References

[1]Weisshaar, T. A., "Aeroelastic Tailoring, Creative Uses of Unusual Materials," *AIAA/ASME/ASCE/AHS 20th Structures, Structural Dynamics, and Materials Conference*, AIAA, Washington, DC, 1987; also AIAA Paper 87-0976, 1987.

[2]Crawley, E. F., "Intelligent Structures for Aerospace: A Technology Overview and Assessment," *AIAA Journal*, Vol. 32, No. 8, 1994, pp. 1689–1699.

[3]Song, O., and Librescu, L., "Free Vibration of Anisotropic Composite Thin-Walled Beams of Closed Cross-Section Contour," *Journal of Sound and Vibration*, Vol. 167, No. 1, 1993, pp. 129–147.

[4]Song, O., and Librescu, L., "Bending Vibration of Cantilevered Thin-Walled Beams Subjected to Time-Dependent External Excitations," *Journal of the Acoustical Society of America*, Vol. 98, No. 1, 1995, pp. 313–319.

[5]Librescu, L., Meirovitch, L., and Song, O., "Refined Structural Modeling for Enhancing Vibrational and Aeroelastic Characteristics of Composite Aircraft Wings," *La Recherche Aerospatiale*, Vol. 1, 1996, pp. 23–35.

[6]Librescu, L., Meirovitch, L., and Song, O., "Integrated Structural Tailoring and Adaptive Materials Control for Advanced Aircraft Wings," *Journal of Aircraft*, Vol. 33, No. 1, 1996, pp. 203–213.

[7]Librescu, L., Meirovitch, L., and Na, S. S., "Control of Cantilever Vibration via Structural Tailoring and Adaptive Materials," *AIAA Journal*, Vol. 35, No. 8, 1997, pp. 1309–1315.

[8]Rehfield, L. W., and Atilgan, A. R., "Toward Understanding the Tailoring Mechanisms for Thin-Walled Composite Tubular Beams," *Proceedings of the First USSR–U.S. Symposium on Mechanics of Composite Materials*, edited by S. W. Tsai, J. M. Whitney, T.-W. Chou and R. M. Jones, American Society of Mechanical Engineers, Fairfield, NJ, 1989, pp. 187–196.

[9]Karpouzian, G., and Librescu, L., "A Comprehensive Model for Anisotropic Composite Aircraft Wings Suitable for Aeroelastic Analyses," *Journal of Aircraft*, Vol. 31, No. 3, 1994, pp. 703–712.

[10]Na, S. S., and Librescu, L., "Oscillation Control of Cantilevers via Smart Materials Technology and Optimal Feedback Control: Actuator Location and Power Consumption Issues," *Analysis and Design Issues for Modern Aerospace Vehicles*, edited by G. J. Simitses, AD-Vol. 55, American Society of Mechanical Engineers, New York, 1997, pp. 231–248.

[11]Yang, J. N., Akbarpour, A., and Ghaemmaghanis, F., "New Control Algorithms for Structural Control," *Journal of Engineering Mechanics*, Vol. 113, No. 12, 1987, pp. 1369–1386.

[12]Soong, T. T., *Active Structural Control: Theory and Practice*, Longman Scientific and Technical, New York, 1990, pp. 75–99.

[13]Chang, M.-Y., "Active Vibration Control of Composite Structures," Ph.D. Thesis, Engineering Science and Mechanics Dept., Virginia Polytechnic Inst. and State Univ., Blacksburg, VA, 1990, pp. 77–83.

[14]Belvin, W. K., and Park, K. C., "Structural Tailoring and Feedback Control Synthesis: An Interdisciplinary Approach," *Journal of Guidance, Control, and Dynamics*, Vol. 13, No. 13, 1997, pp. 424–429.

[15]Helgeson, R. J., and Szustak, P. W., "Saturation Constrained LQR," *Tenth Symposium on Structural Dynamics and Control*, edited by L. Meirovitch, Virginia Polytechnic Inst. and State Univ. Blacksburg, VA, 1995, pp. 25–36.

[16]Khot, N. S., Veley, D. E., and Bolonkin, A. A., "Design of Smart Structures with Bounded Controls," *Smart Structures and Materials 1996; Mathematics and Control in Smart Structures*, edited by V. Varadan and J. Chandra, Proceedings of SPIE 2715, International Society for Optical Engineering, Bellingham, Washington, 1996, pp. 173–183.

[17]Bailey, T., and Hubbard, J. E., Jr., "Distributed Piezoelectric-Polymer Active Vibration Control of a Cantilever Beam," *Journal of Guidance, Control, and Dynamics*, Vol. 8, No. 5, 1985, pp. 605–611.

[18]Dosch, J. J., Inman, D. J., and Garcia, E., "A Self-Sensing Piezoelectric Actuator for Collocated Control," *Journal of Intelligent Material Systems and Structures*, Vol. 3, No. 1, 1992, pp. 166–184.

[19]Sunar, M., and Rao, S. S., "Distributed Modeling and Actuator Location for Piezoelectric Control Systems," *AIAA Journal*, Vol. 34, No. 10, 1996, pp. 2209–2211.

[20]Librescu, L., and Nosier, A., "Response of Shear Deformable Elastic Laminated Composite Flat Panels to Sonic Boom and Explosive Blast Loadings," *AIAA Journal*, Vol. 28, No. 2, 1990, pp. 345–352.

[21]Librescu, L., and Na, S. S., "Dynamic Response of Cantilevered Thin-Walled Beams to Blast and Sonic Boom Loadings," *Journal of Shock and Vibration*, Vol. 5, No. 1, 1998, pp. 23–33.